



Inclined Lorentzian force effect on tangent hyperbolic radiative slip flow imbedded carbon nanotubes: Lie group analysis

P. Sreenivasulu^a, B. Vasu^{b,*}, T. Poornima^c and N. Bhaskar Reddy^d

^aDepartment of Mathematics, Sri Venkateswara Engineering College for Women, Tirupati, A.P., 517502, India.

^bDepartment of Mathematics, Motilal Nehru National Institute of Technology, Allahabad, U. P. -211004, India

^cDepartment of Mathematics, SAS, VIT University, Vellore, T.N, India.

^dDepartment of Mathematics, S.V. University, Tirupati-517502, A. P., India.

Article info:

Type: Research
Received: 08/10/2018
Revised: 17/10/2018
Accepted: 27/10/2018
Online: 27/10/2018

Keywords:

Aligned Lorentzian force,
Navier slip,
Thermal slip,
Carbon nanotubes,
Lie group analysis.

Abstract

The present paper focuses on a numerical study for an inclined magneto-hydrodynamic effect on free convection flow of a tangent hyperbolic nanofluid embedded with carbon nanotubes (CNTs) over a stretching surface taking velocity and thermal slip into account. Two types of nanoparticles are considered for the study; they are single and multi-walled nanotubes. The presentation of single-parameter group (Lie group) transformations reduce the independent variable number by one, and hence the partial differential governing equations with the supplementary atmospheres into an ordinary differential equation with the appropriate suitable conditions. The obtained ordinary differential equations are then numerically solved by employing the fourth-order Runge-Kutta technique along with the shooting method. The effects of the various parameters governing the flow field are presented with the help of graphs. The investigation reveals that the non-Newtonian MWCNTs Tangent hyperbolic nano-liquid reduces the friction near the stretching sheet contrasting SWCNTs. This combination can be used as a friction lessening agent/factor. The usage of CNTs shows an excellent performance in enhancing the thermal conductivity of the nanofluid and that single-wall carbon nanotubes (SWCNTs) have a higher thermal conductivity in comparison to multi-wall carbon nanotubes (MWCNTs) even in the presence of radiative heat transfer and heat source. The comparison with existing results available in the literature is made and had an excellent coincidence with our numerical method.

1. Introduction

Warmth exchange in the recent era has become an inevitable one as increased productivity of compact objects. This warmth exchange liquid assumes a key part in the advancement of vitality proficient warmth exchange hardware including

electrons, transportation and HVAC & R. The role of nanomaterials has turned top in handling such type of products. The non-Newtonian nanofluids groups better long haul solidness and rheological properties when contrasted with millimeter or micrometer measured molecule suspensions. Nanotubes are from the fullerene

*Corresponding author
email address: bvasu@mnit.ac.in

auxiliary family and it is received from beneficiary long and empty structure with the divider composed by one particle thick sheets of carbon, called graphene. Carbon nanotubes are characterized into single or multi-walled carbon nanotubes. The investigation of carbon nanotubes (CNTs) started in 1991, and it is opened up another period in materials science. These are the mind boggling structures that have a variety of intriguing electronic, attractive and mechanical properties. CNT is no less than 100 times more grounded than steel, however just a single 6th as substantial, so nanotube fibers could reinforce any material. Nanotubes warm conductivity is superior to copper. CNTs are prior utilized as a part of polymers to control or upgrade conductivity and are added to hostile to static bundling. CNTs have different structures, contrasting in thickness, length and number of layers. The physical attributes of nanotubes are distinctive relying upon how the graphene sheet is moved up from the tube starting it to act either metallic or a semiconductor. CNTs have various applications, for example, controlling the warm conductivity, field outflow, conductive properties, vitality stockpiling and conductive glue, atomic gadgets in light of CNTs, warm materials and basic outlining. Choi [1], investigated that the nanofluid is now one of the fastest growth rates in scientific papers in nanoscale science and technology. Chandrasekhar and Kasi [2] analyzed the heat and mass transfer effects on MHD nanofluid. Hayat et al. [3] discussed MHD nanofluid with power law velocity and chemical reaction. Gorla and Vasu [4] studied unsteady convective heat transfer to a stretching surface in a non-Newtonian nanofluid. Kameswaran et al. [5] studied numerically the convective heat transfer in the influence of non-linear Boussinesq approximation, thermal stratification and convective boundary conditions on non-Darcy nanofluid flow over a vertical wavy surface. Rizwan et al. [6] presented the thermo-physical effects of carbon nanotubes on MHD flow past a stretching sheet. Waqar et al. [7] studied the analysis of heat transfer on MHD water functionalized carbon nanotubes past a static/moving wedge. Khan et al. [8] investigated the effect of heat transfer with

carbon nanotubes past a flat surface in the presence of Navier slip. The slip flow and convective heat transfer in MHD carbon of a nanotube over a stretching surface was studied by Rizwan et al. [9].

The stream and heat exchange along with magnetohydrodynamic has pulled in the consideration of numerous specialists due to the significance of the attractive impact on the limit layer control; the liquid stream and its applications are essential in numerous building issues, for example, atomic reactors, MHD generators, plasma contemplates and geothermal vitality extractions and so on. Haq et al. [10] studied thermophysical effects of carbon nanotubes on MHD flow past a stretching sheet. Magnetohydrodynamic convective boundary layer flow of dissipating nanofluid past an exponential stretching sheet was presented by Sreenivasulu and Poornima [11]. Poornima et al. [12] analysed the effect of temperature dependent viscosity on mixed convection MHD dissipating cylindrical shaped Cu-water nanofluid flow over a vertical moving surface. Hayat et al. [13] analysed the Powell-Eyring MHD nanofluid flow over a non-linear stretching surface with variable thickness. Beg et al. [14] presented computational solutions for steady-state boundary layer flow of a nanofluid from an impermeable vertical flat wall in a porous medium saturated with a water-based dilute nanofluid containing oxytactic microorganisms. Reddy et al. [15] studied the flow and heat transfer characteristics of Williamson MHD Nanofluid over a stretching surface in the presence of variable thermal conductivity and variable thickness. Electrically magnetic field applied transversely normal to the fluid flow aligned is studied under Maxwell's law. This part has wide applications in the power generators, magnetic shielding, bearings, and electrically leading fluid. An aligned magnetic effect on plasma structures was explained by Ergun et al. [16].

The study of thermal radiation and heat transfer is of great importance whenever the environment is at higher temperature and its applications play an important role in the design of various advanced thermal conversion system having high temperature. Rashidi et al. [17]

explained the radiative effect on MHD nanofluid. Wahed and Akl [18] studied the hall current effect on MHD nanofluid with non-linear thermal radiation. Lu et al. [19] elucidated the non-linear thermal radiation effect on MHD Williamson nanofluid with constant wall temperature. Poornima et al. [20] proposed the slip flow of Casson rheological fluid under variable thermal conductivity and thermal radiation. Bhaskar Reddy et al. [21] investigated the effect of radiation on MHD slip flow of nanofluid over an exponential porous stretching sheet with viscous dissipation. Radiation influence on MHD Williamson nanofluid was studied by Kho et al. [22]. Boundary layer MHD convective flow of EG based Cu nanotubes past an extensible moving surface with thermal radiation was presented by Poornima and Sreenivasulu [23]. A radiation effect in stagnation point flow on carbon water nanofluid was presented by Hayat et al. [24]. Rashid et al. [25] explained the effect of radiation on water based metallic nanoparticles with prescribed surface temperature.

The tangent hyperbolic fluid model is enough competent to describe shear thinning phenomenon. It measures the fluid sustaining less flow with more rate of shear stress. Examples of the fluids having this property are ketchup, paint, blood etc. In literature many studied were reported on tangent hyperbolic fluid by considering different physical aspects. An important branch of the non-Newtonian fluid models is the hyperbolic tangent fluid model. The hyperbolic tangent fluid is used extensively for different laboratory experiments. Hussain et al. [26] discussed the dissipative impact on tangent hyperbolic flow under convective boundary condition. Zakir and Zaman [27] studied the MHD tangent hyperbolic flow past a stretching sheet with slip employing Lie group analysis. Akbar et al. [28] numerically analyzed the MHD tangent hyperbolic flow towards stretching sheet. Thammanna et al. [29] investigated combined effects of partial slip and Ohmic heating on MHD nanoflow. Naseer et al. [30] analyzed hyperbolic tangent flow over an exponential expanding cylinder. Sandeep [31] studied the aligned Lorentzian force on thin nano-film suspended graphene particles. Sailaja

et al. [32] explained the influence of aligned magnetic field over Casson film flow. Arifin et al. [33] described the aligned MHD effect past a two-phase dusty Casson flow with Newtonian heating. Rashidi et al. [34] discussed the squeezing flow between parallel plates under inclined magnetic field effect. Waini et al. [35] studied inclined Lorentz force effect on UCM fluid with stretching /shrinking of sheet. Ashwin kumar et al. [36] presented the effect of the aligned magnetic field on MHD nanoflow over a semi-infinite vertical plate with ferrous nanoparticles.

Motivated by the above-mentioned studies, the objective of the present study is to examine the Lie group analysis for the radiation and slip effects on boundary layer flow of carbon nanofluids with aligned magnetic field and heat generation /absorption.

2. Mathematical model

A steady two-dimensional boundary layer flow of an incompressible tangent hyperbolic fluid flow of a nanofluid past a stretching sheet with aligned magnetic field and partial slip is considered. The flow is considered along the \bar{x} -axis, which is taken along the stretching surface, and the \bar{y} -axis is taken perpendicular to sheet (Fig. 1). The flow is conformed to $\bar{y} > 0$. The surface of the plane is maintained at a constant temperature T_w higher than the constant temperature T_∞ of the ambient nanofluid. The fluid is a water based nanofluid containing two kinds of nanotubes such as single-wall carbon nanotubes (SWCNTs) and multi-wall carbon nanotubes (MWCNTs). The nanofluid is assumed incompressible and the flow is assumed to be laminar. The thermophysical properties of the nanofluid are given in Table 1.

The constitutive equation for hyperbolic tangent fluid model is given by [28]:

$$\bar{\tau} = \left[\mu_\infty + (\mu_0 + \mu_\infty) \tanh(\Gamma \bar{\gamma})^n \right] \bar{\gamma} \quad (1)$$

where $\bar{\tau}$ is the extra stress tensor, μ_0 is the zero shear rate viscosity, μ_∞ is the infinite shear rate viscosity, Γ is the time dependent material

constant and n is the flow behaviour index. The term $\bar{\gamma}$ can be expressed as:

$$\bar{\gamma} = \sqrt{\frac{1}{2} \sum_i \sum_j \bar{\gamma}_{ij} \bar{\gamma}_{ij}} = \sqrt{\frac{1}{2} \Pi} \quad (2)$$

where $\Pi = \frac{1}{2} tr \left(gradV + (gradV^T) \right)^2$. As the infinite shear rate viscosity problem is concerned, so in the following, it is restricted to the case $\mu_\infty = 0$. The fluid under consideration described shear thinning, so $\Gamma \bar{\gamma} < 1$ must be taken. Then Eq. (1) reduces to:

$$\begin{aligned} \bar{\tau} &= \mu_0 \left[(\Gamma \bar{\gamma})^n \right] \bar{\gamma} = \mu_0 \left[(1 + \Gamma \bar{\gamma} - 1)^n \right] \bar{\gamma} \\ &= \mu_0 \left[(1 + n(\Gamma \bar{\gamma} - 1))^n \right] \bar{\gamma} \end{aligned} \quad (3)$$

The boundary layer and Boussinesq approximations are assumed to be valid. Under these assumptions, the governing boundary layer equations can be written in a dimensional form as:

Table 1. Thermal properties of base fluid and nanoparticles [8].

| Physical properties | Base fluid | | Nanoparticles | |
|---|------------|------------------------------|-----------------------------|--|
| | Water | Single-wall carbon nanotubes | Multi-wall carbon nanotubes | |
| ρ (kg/m ³) | 997 | 2600 | 1600 | |
| C_p (J/kg K) | 4179 | 425 | 796 | |
| k (W/m K) | 0.613 | 6600 | 3000 | |
| $\beta \times 10^{-5}$ (K ⁻¹) | 21 | 0.33 | 0.72 | |

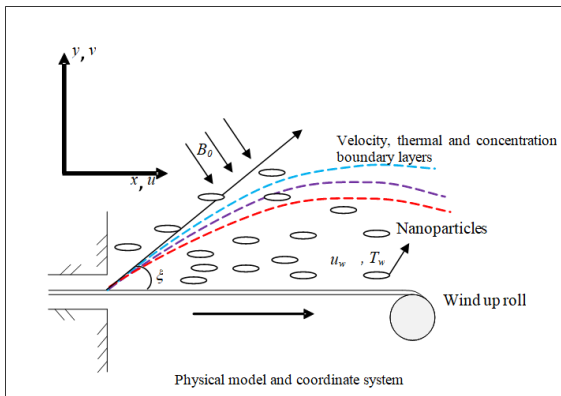


Fig. 1. Physical model and flow configuration.

$$\frac{\partial \bar{u}}{\partial \bar{x}} + \frac{\partial \bar{v}}{\partial \bar{y}} = 0 \quad (4)$$

$$\begin{aligned} \bar{u} \frac{\partial \bar{u}}{\partial \bar{x}} + \bar{v} \frac{\partial \bar{u}}{\partial \bar{y}} &= \frac{1}{\rho_{nf}} [\mu_{nf} (1-n) \frac{\partial^2 \bar{u}}{\partial \bar{y}^2} + \\ &\sqrt{2} n \Gamma \left(\frac{\partial u}{\partial y} \right) \frac{\partial^2 u}{\partial y^2} - \sigma B_0^2 \sin^2(\xi) \bar{u}] \end{aligned} \quad (5)$$

$$\begin{aligned} \bar{u} \frac{\partial T}{\partial \bar{x}} + \bar{v} \frac{\partial T}{\partial \bar{y}} &= \alpha_{nf} \frac{\partial^2 T}{\partial \bar{y}^2} - \frac{1}{(\rho C_p)_{nf}} \frac{\partial q_r}{\partial \bar{y}} \\ &+ \frac{Q_0}{(\rho C_p)_{nf}} (T - T_\infty) \end{aligned} \quad (6)$$

where \bar{u} and \bar{v} are velocity components in the \bar{x} and \bar{y} directions, T is the local Temperature of the nano fluid, g is the acceleration due to gravity, σ is the electric conductivity, B_0 is the uniform magnetic field strength, ρ_{nf} is the effective density of the nanofluid, μ_{nf} is the effective dynamic viscosity of the nanofluid and α_{nf} is the thermal diffusivity of the nanofluid, q_r is the radiative heat flux and Q_0 is the volumetric rate of heat generation.

Boundary conditions of these equations are:

$$\begin{aligned} \bar{u} &= \bar{u}_w(\bar{x}) + N \frac{\partial \bar{u}}{\partial \bar{y}}, \bar{v} = \bar{v}_w, T = T_w + L \frac{\partial T}{\partial \bar{y}} \text{ at } \bar{y} = 0 \\ \bar{u} &\rightarrow 0, \quad T \rightarrow T_\infty \quad \text{as } \bar{y} \rightarrow \infty \end{aligned} \quad (7)$$

where $\bar{u}_w(\bar{x}) = a \bar{x}$ is the stretching velocity.

The Rosseland approximation for radiative heat flux is:

$$q_r = -\frac{4}{3} \frac{\sigma^*}{k^*} \frac{\partial T^4}{\partial \bar{y}} \quad (8)$$

where σ^* is the Stefan-Boltzmann constant and k^* is the mean absorption coefficient. If the temperature differences within the flow are adequately small, then Eq. (5) can be linearized by expanding T^4 into the Taylor series about T_∞ after ignoring the higher-order terms:

$$T^4 \cong 4T_\infty^3 T - 3T_\infty^4 \quad (9)$$

In the sight of Eqs. (8 and 9), Eq. (6) becomes:

$$\bar{u} \frac{\partial T}{\partial \bar{x}} + \bar{v} \frac{\partial T}{\partial \bar{y}} = \alpha_{nf} \left(1 + \frac{4}{3} R \right) \frac{\partial^2 T}{\partial \bar{y}^2} + \frac{Q_0}{(\rho C_p)_{nf}} (T - T_\infty) \quad (10)$$

where $R = 16\sigma^* T_\infty^3 / 3k_f k^*$ is the radiation constraint.

Several researchers projected that nanofluid models are effective only for spherical or rotational elliptical particles with small axial ratio and these models do not describe the properties of space distribution of the carbon nanotubes on thermal conductivity. Nevertheless the carbon nanotubes can be regarded as rational elliptical model with large axial ratio. A theoretical model based on Maxwell theory including rotational elliptical nanotubes with very large axial ratio and reimbursing the effects of space distributions on carbon nanotubes (CNTs) was proposed by Xue [37].

$$\rho_{nf} = (1 - \phi)\rho_f + \phi\rho_{CNT}, \quad \alpha_{nf} = \frac{k_{nf}}{(\rho C_p)_{nf}},$$

$$(\rho C_p)_{nf} = (1 - \phi)(\rho C_p)_f + \phi(\rho C_p)_{CNT},$$

$$\frac{k_{nf}}{k_f} = \frac{1 - \phi + 2\phi \frac{k_{CNT}}{k_{CNT} - k_f} \ln \frac{k_{CNT} + k_f}{2k_f}}{1 - \phi + 2\phi \frac{k_f}{k_{CNT} - k_f} \ln \frac{k_{CNT} + k_f}{2k_f}},$$

$$(\rho\beta)_{nf} = (1 - \phi)(\rho\beta)_f + \phi(\rho\beta)_{CNT},$$

$$\mu_{nf} = \frac{\mu_f}{(1 - \phi)^{2.5}} \quad (11)$$

where ϕ is the solid volume fraction of nanotubes. Here the subscripts nf, f and CNT represent the thermo physical properties of the nanofluids, base fluid and nano-solid particles respectively.

The following non-dimensional variables is introduced:

$$x = \sqrt{\frac{a}{v_f}} \bar{x}, y = \sqrt{\frac{a}{v_f}} \bar{y}, u = \frac{\bar{u}}{\sqrt{av_f}}, \quad (12)$$

$$v = \frac{\bar{v}}{\sqrt{av_f}}, \theta = \frac{T - T_\infty}{T_w - T_\infty}.$$

Eqs. (4, 5 and 10) take the subsequent non-dimensional form:

$$\frac{\partial u}{\partial x} + \frac{\partial v}{\partial y} = 0 \quad (13)$$

$$u \frac{\partial u}{\partial x} + v \frac{\partial u}{\partial y} = \frac{1}{(1 - \phi + \phi\rho_{CNT} / \rho_f)}$$

$$\left\{ \frac{1}{(1 - \phi)^{2.5}} (1 - n) \frac{\partial^2 u}{\partial y^2} + \sqrt{2n} \Gamma a \left(\frac{\partial u}{\partial y} \right) \frac{\partial^2 u}{\partial y^2} - \text{Sin}^2 \xi M u \right\} \quad (14)$$

$$u \frac{\partial \theta}{\partial x} + v \frac{\partial \theta}{\partial y} = \frac{1}{\text{Pr} [1 - \phi + \phi(\rho C_p)_{CNT} / (\rho C_p)_f]} \left(1 + \frac{4}{3} R \right) \left(\frac{k_{nf}}{k_f} \right) \frac{\partial^2 \theta}{\partial y^2} + \frac{\lambda}{[1 - \phi + \phi(\rho C_p)_{CNT} / (\rho C_p)_f]} \theta \quad (15)$$

With the corresponding boundary conditions:

$$u = x + \sqrt{\frac{a}{v_f}} N \frac{\partial u}{\partial y}, v = \sqrt{av_f} v_w, \left. \begin{aligned} & \theta = 1 + \sqrt{\frac{a}{v_f}} L \frac{\partial \theta}{\partial y} \end{aligned} \right\} \text{at } y = 0 \quad (16)$$

$$u \rightarrow 0, \quad \theta \rightarrow 0 \quad \text{as } y \rightarrow \infty$$

where $\text{Pr} = v_f / \alpha_f$ is the Prandtl number $\lambda = Q_0 / a(\rho C_p)_f$ is the coefficient of heat generation/absorption and $M = \sigma B_0^2 / \rho_f a$ is the magnetic parameter.

By presenting the stream function ψ , which is defined by $u = \partial \psi / \partial y$ and $v = -\partial \psi / \partial x$ the system (14) and (15) becomes:

$$\frac{\partial \psi}{\partial y} \frac{\partial^2 \psi}{\partial x \partial y} - \frac{\partial \psi}{\partial x} \frac{\partial^2 \psi}{\partial y^2} = \frac{1}{(1-\phi + \phi \rho_{CNT} / \rho_f)} \left\{ \begin{aligned} &\frac{1}{(1-\phi)^{2.5}} (1-n) \frac{\partial^3 \psi}{\partial y^3} + \\ &\sqrt{2n} \Gamma a \left(\frac{\partial \psi}{\partial y} \right) \frac{\partial^3 \psi}{\partial y^3} - M \text{Sin}^2 \xi \frac{\partial \psi}{\partial y} \end{aligned} \right\} \quad (17)$$

$$\frac{\partial \psi}{\partial y} \frac{\partial \theta}{\partial x} - \frac{\partial \psi}{\partial x} \frac{\partial \theta}{\partial y} = \frac{1}{\text{Pr} [1-\phi + \phi(\rho Cp)_{CNT} / (\rho Cp)_f]} \left(1 + \frac{4}{3} R \right) \left(\frac{k_{nf}}{k_f} \right) \frac{\partial^2 \theta}{\partial y^2} + \frac{\lambda}{[1-\phi + \phi(\rho Cp)_{CNT} / (\rho Cp)_f]} \theta \quad (18)$$

with the boundary conditions:

$$\left. \begin{aligned} \frac{\partial \psi}{\partial y} &= x + \sqrt{\frac{a}{v_f}} N \frac{\partial^2 \psi}{\partial y^2}, \\ \frac{\partial \psi}{\partial x} &= -\sqrt{a v_f} v_w, \theta = 1 + \sqrt{\frac{a}{v_f}} L \frac{\partial \theta}{\partial y} \end{aligned} \right\} \text{at } y=0 \quad (19)$$

$u \rightarrow 0, \quad \theta \rightarrow 0 \quad \text{as } y \rightarrow \infty$

3. Lie group analysis

The simplified form of Lie-group transformations namely, the scaling group of transformations (Mukhopadhyay et al. [38]) is now introduced.

$$\Gamma_1 : x^* = x e^{\epsilon \alpha_1}, y^* = y e^{\epsilon \alpha_2}, \psi^* = \psi e^{\epsilon \alpha_3}, \theta^* = \theta e^{\epsilon \alpha_4} \quad (20)$$

Substituting Eq. (20) in Eqs. (17 and 18):

$$e^{\epsilon(\alpha_1 + 2\alpha_2 - 2\alpha_3)} \left(\frac{\partial \psi^*}{\partial y^*} \frac{\partial^2 \psi^*}{\partial x^* \partial y^*} - \frac{\partial \psi^*}{\partial x^*} \frac{\partial^2 \psi^*}{\partial y^{*2}} \right) = \frac{1}{(1-\phi + \phi \rho_{CNT} / \rho_f)} \left\{ \begin{aligned} &\frac{(1-n)}{(1-\phi)^{2.5}} e^{\epsilon(3\alpha_2 - \alpha_3)} \frac{\partial^3 \psi^*}{\partial y^{*3}} + \\ &e^{\epsilon(5\alpha_2 - 2\alpha_3 - \alpha_5)} \sqrt{2n} \Gamma a^* \frac{\partial^2 \psi^*}{\partial y^{*2}} \frac{\partial^3 \psi^*}{\partial y^{*3}} \\ &- M e^{\epsilon(\alpha_2 - \alpha_3)} \frac{\partial \psi^*}{\partial y^*} \end{aligned} \right\} \quad (21)$$

$$e^{\epsilon(\alpha_1 + \alpha_2 - \alpha_3 - \alpha_4)} \left(\frac{\partial \psi^*}{\partial y^*} \frac{\partial \theta^*}{\partial x^*} - \frac{\partial \psi^*}{\partial x^*} \frac{\partial \theta^*}{\partial y^*} \right) = \frac{1}{\text{Pr} [1-\phi + \phi(\rho Cp)_{CNT} / (\rho Cp)_f]} \left(1 + R \right) \left(\frac{k_{nf}}{k_f} \right) e^{\epsilon(2\alpha_2 - \alpha_4)} \frac{\partial^2 \theta^*}{\partial y^{*2}} + \frac{\lambda}{\text{Pr} [1-\phi + \phi(\rho Cp)_{CNT} / (\rho Cp)_f]} e^{-\epsilon \alpha_4} \theta^* \quad (22)$$

The system of equations will remain unchanged under the group of transformations Γ_1 , and the following families among the parameters can be obtained:

$$\begin{aligned} \alpha_1 + 2\alpha_2 - 2\alpha_3 &= 3\alpha_2 - \alpha_3 \\ &= 5\alpha_2 - 2\alpha_3 - \alpha_5 = \alpha_2 - \alpha_3 \\ \alpha_1 + \alpha_2 - \alpha_3 - \alpha_4 &= 2\alpha_2 - \alpha_4 = -\alpha_4 \end{aligned}$$

These relations give:

$$\alpha_3 = \alpha_1, \alpha_2 = \alpha_4 = 0 \text{ and } \alpha_5 = -\alpha_1$$

The set of transformations of the Γ_1 group reduces to:

$$\Gamma_1 : x^* = x e^{\epsilon \alpha_1}, y^* = y, \psi^* = \psi e^{\epsilon \alpha_1}, \theta^* = \theta, \Gamma^* = \Gamma_p e^{-\epsilon \alpha_1} \quad (23)$$

Expanding (20) in power of ε by Taylor's technique and keeping terms up to the order of ε :

$$\begin{aligned} x^* - x &= x\varepsilon\alpha_1, y^* - y = 0, \psi^* - \psi = \psi\varepsilon\alpha_1, \\ \theta^* - \theta &= \theta\varepsilon\alpha_1, \Gamma^* - \Gamma_p = -\Gamma_p\varepsilon\alpha_1 \end{aligned} \tag{24}$$

The characteristic functions are:

$$\frac{dx}{x\alpha_1} = \frac{dy}{0} = \frac{d\psi}{\psi\alpha_1} = \frac{d\theta}{0} = \frac{d\Gamma_p}{-\Gamma_p\alpha_1} \tag{25}$$

from which, the following similarity variables are obtained:

$$\begin{aligned} \eta &= y^*, \psi^* = x^* f(\eta), \\ \theta^* &= \theta(\eta), \Gamma_p^* = \frac{1}{x^*} \Gamma_0 \end{aligned} \tag{26}$$

With the help of these relations, the Eqs. (21 and 22) become:

$$(1-n)f''' + (1-\phi)^{2.5} \left\{ \left[1 - \phi + \phi(\rho_{CNT} / \rho_f) \right] (ff'' - (f')^2) \right\} = 0 \tag{27}$$

$$\left(1 + \frac{4}{3}R \right) \left(\frac{k_{nf}}{k_f} \right) \theta'' + Pr \tag{28}$$

$$[(1 - \phi + \phi(\rho_{CNT} / \rho_f)) f\theta' + \lambda\theta] = 0$$

The agreeing boundary conditions (19) become:

$$\begin{aligned} f'(0) &= 1 + \beta f''(0), f(0) = S, \\ \theta(0) &= 1 + \delta\theta'(0) \\ f'(\infty) &\rightarrow 0, \quad \theta(\infty) \rightarrow 0 \end{aligned} \tag{29}$$

where $\beta = \sqrt{a/v_f}N$ is the velocity slip parameter, $S = -\sqrt{av_f}v_w$ is the suction/injection parameter, $\delta = \sqrt{a/v_f}L$ is the temperature slip parameter and $W_e = \sqrt{2}\Gamma a$ be the Weissenberg number.

The skin friction coefficient C_f and the Nusselt number Nu_x , which are defined as:

$$\begin{aligned} C_f &= \frac{\mu_{nf}}{\rho_f u_w^2} \left[(1-n) \left(\frac{\partial \bar{u}}{\partial \bar{y}} \right)_{\bar{y}=0} + \frac{n\Gamma}{\sqrt{2}} \left(\frac{\partial \bar{u}}{\partial \bar{y}} \right)_{\bar{y}=0}^2 \right], \\ Nu_x &= \frac{\bar{x}k_{nf}}{k_f(T_w - T_\infty)} \left(-\frac{\partial T}{\partial \bar{y}} \right)_{\bar{y}=0} \end{aligned} \tag{30}$$

Using the Eqs. (8, 24 and 27), the coefficient of skin friction and local Nusselt number are described as:

$$\begin{aligned} Re_x^{1/2} C_f &= \frac{1}{(1-\phi)^{2.5}} \left[(1-n)f''(0) + \frac{n}{2} W_e (f''(0))^2 \right], \\ Re_x^{-1/2} Nu_x &= -\frac{k_{nf}}{k_f} \theta'(0) \end{aligned} \tag{31}$$

where $Re_x = \bar{u}_w(\bar{x})\bar{x} / \nu_f$ is the local Reynolds number.

4. Results and discussion

The coupled non linear representing boundary layer Eqs. (24) and (25) subjected to the boundary conditions (26) is explained numerically by utilizing fourth request Runge-Kutta strategy alongside shooting technique. First of all higher order non-linear equations are converted into simultaneous linear differential equations of first order and then transformed into an initial value problem by applying the shooting method. The resultant initial problem is solved by employing fourth order Runge-Kutta technique. A representative set of numerical results are presented graphically in Figs. 2–22. In order to assess the accuracy of numerical calculation, the present results for skin friction values are compared with the special case of Uma Maheswar Rao and KoteswaraRao [39] and Akbar et al. [28] and Ullah and Zaman [27] and found that the present results are in excellent agreement (Tables 2 and 3).

Table 2. Comparison results of surface skin friction for a particular case [39].

| N | We | M | Uma Maheswara Rao and Koteswara rao [39] | Present study |
|-----|-----|-----|--|---------------|
| 0.1 | | | 1.15892610 | 1.15893122 |
| 0.3 | | | 1.01304949 | 1.01303861 |
| 0.5 | 0.1 | | 0.83768770 | 0.83768767 |
| | 0.5 | | 1.14675023 | 1.14674032 |
| | 1.0 | 0.5 | 1.13077886 | 1.13077645 |
| | | 1.0 | 1.33774399 | 1.33774398 |
| | | 2.0 | 1.63740820 | 1.63772102 |

Iteration of velocity and temperature profile with nanoparticles volume fraction of CNTs is depicted in Figs. 2 and 3; it is noticed that the warmth of the fluid is an elevating function of ϕ for both types of CNTs. Physically, the logic is an increase in thermal conductivities of nanofluids due to supplement of more CNTs.

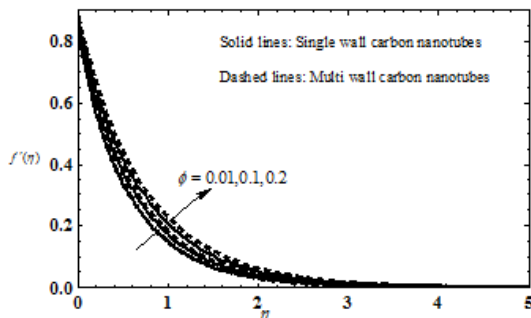


Fig. 2. Velocity profiles for different values of ϕ .

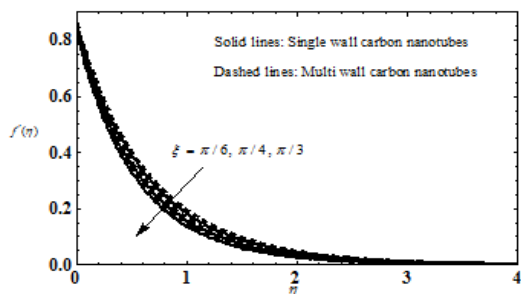


Fig. 4. Velocity profiles for different values of ξ .

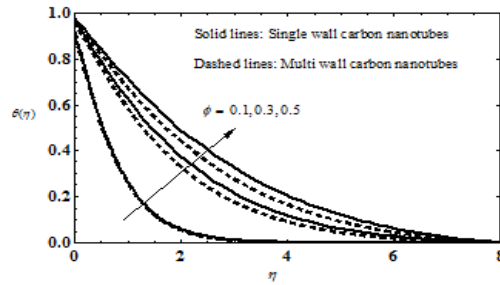


Fig. 3. Temperature profiles for different values of ϕ .

The more the volume fraction of CNTs in the nanofluids, the more will be its thermal conductivity which in turn enhances the temperature of the fluids. By maximizing the volume fraction ϕ of CNTs, a gradual elevation is observed in thermal conductivity. Fig. 2 shows that there is an elevation in the velocity of the fluid for escalating ϕ values. The impact of ϕ on the flow of Maxwell nanofluid: it is spotted that velocity profile maximizes with increasing ϕ for both type of CNTs (SWCNT and MWCNT).

The impact of aligned magnetic on $f'(\eta)$ and $\theta(\eta)$ (Figs. 4 and 5): it is spotted that elevation in aligned magnetic parameter drops the velocity profiles and swifts the temperature profiles. This may happen due to the reason that an increase angle varying magnetic field strengthens the applied magnetic field.

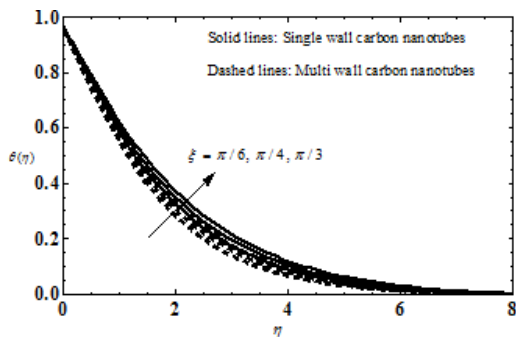


Fig. 5. Temperature profiles for different values of ξ .

Table 3. Comparison results of surface skin friction for some particular cases.

| n | M | Akbar et al [28] | | | Zakir Ullah, Gul Zaman [27] | | | Present study | | |
|-----|-----|------------------|---------|---------|-----------------------------|---------|---------|---------------|---------|---------|
| | | We=0.0 | We=0.3 | We=0.5 | We=0.0 | We=0.3 | We=0.5 | We=0.0 | We=0.3 | We=0.5 |
| 0.0 | 0.0 | 1 | 1 | 1 | 1 | 1 | 1 | 1 | 1 | 1 |
| 0.1 | 0.0 | 0.94868 | 0.94248 | 0.93826 | 0.94868 | 0.94248 | 0.93826 | 0.94860 | 0.94252 | 0.93321 |
| 0.2 | 0.0 | 0.89442 | 0.88023 | 0.87026 | 0.89442 | 0.88023 | 0.87026 | 0.89438 | 0.88019 | 0.87023 |
| 0.3 | 0.5 | 1.09544 | 0.98804 | 0.96001 | 1.02472 | 0.98804 | 0.96001 | 1.09551 | 0.98806 | 0.96032 |
| 0.3 | 1.0 | 1.26491 | 1.13454 | 1.09616 | 1.18322 | 1.13454 | 1.09616 | 1.26490 | 1.13448 | 1.09609 |
| 0.3 | 1.5 | 1.41421 | 1.26193 | 1.21235 | 1.32288 | 1.26193 | 1.21235 | 1.41423 | 1.26189 | 1.21229 |

Quite commonly, increasing magnetic field parameter generates a resistive type of force to the tangent hyperbolic nano fluid flow, called drag force or Lorentzian force. This energy has the capacity to recede the movement of the nanoliquid for both types of CNTs. Although, it is seen that MWCNT velocity profiles elevates more than SWCNTs. Interestingly, the thermal boundary layer thickens, rising the warmth in the nanoliquid. SWCNTs have higher rate of heat transfer than MWCNTs at the same volume fraction. It is due to the fact that SWCNT has greater thermal conductivity than MWCNT.

Influence of suction/injection parameter on $f'(\eta)$ and $\theta(\eta)$ (Figs. 6 and 7): it is detected that from these graphs the velocity of CNTs based nanofluid declines continuously with increase in suction/injection parameter, for all values of η (Fig. 6). MWCNTs velocity profiles have higher rate of values than SWCNTs distribution for same suction/injection variation. Similarly temperature profiles also decreases as rising suction/injection values (Fig. 7). It is due to the fact that SWCNT has greater thermal conductivity than MWCNT. The enhancement of heat in the nanofluid for SWCNT is higher than that of MWCNTs. It is due to the fact that SWCNT has greater thermal conductivity than MWCNT.

Power law index ratio effect on $f'(\eta)$ and $\theta(\eta)$ (Figs. 8 and 9): it is quite fascinating to observe that for accelerating power law index n , the momentum boundary layer thickness reduces showing a deceleration in the velocity profiles for both type of CNTs. But the thickness of the thermal boundary layer increases for increasing n values. Thus the heat in the fluid rises up.

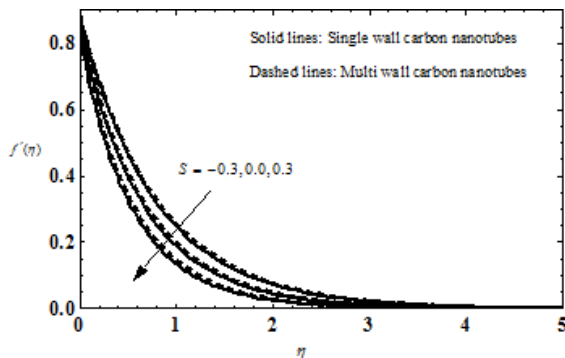


Fig. 6. Velocity profiles for different values of S.

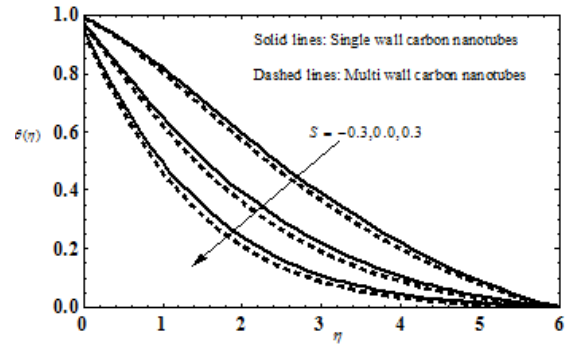


Fig. 7. Temperature profiles for different values of S.

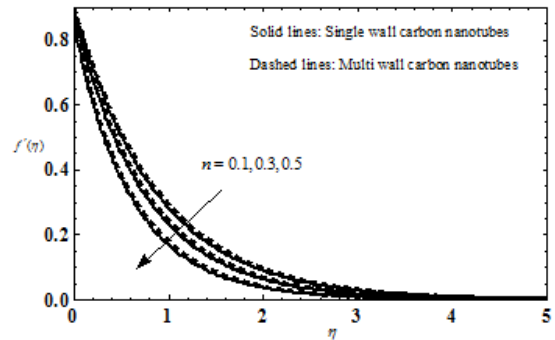


Fig. 8. Velocity profiles for different values of n.

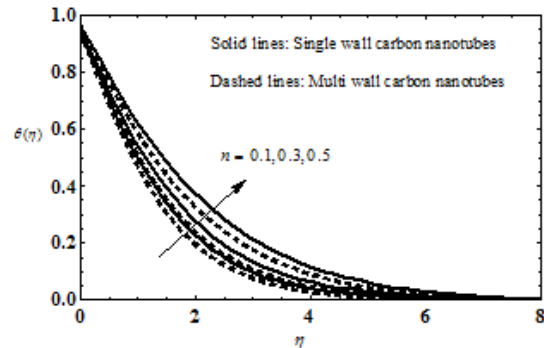


Fig. 9. Temperature profiles for different values of n.

Consequence of strengthening fluid parameter We on $f\eta(\cdot)$ and $\eta(\theta)$ (Figs. 10 and 11): the influence of Weissenberg number on velocity profile is portrayed in Fig. 10,. Escalating We values recedes the momentum of the fluid since the fluid parameter is the ratio of relaxation time over process time. So, strengthening the fluid parameter implies enhancing the relaxation time, this in turn resists the flow and hence velocity reduces for both types of nanoparticles. Moreover, multi-walled nanotubes show a better performance in comparison to single-walled particles. While the thermal boundary layer thickens, the heat in the nanoliquid enhances.

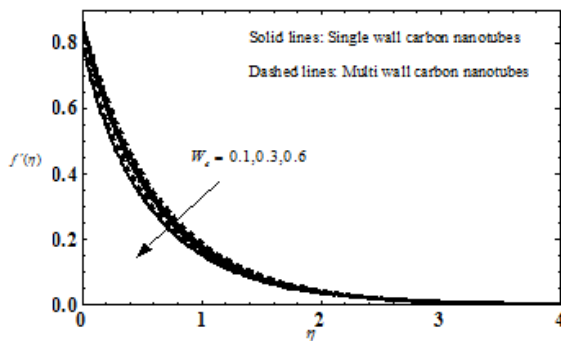


Fig. 10. Velocity profiles for different values of We .

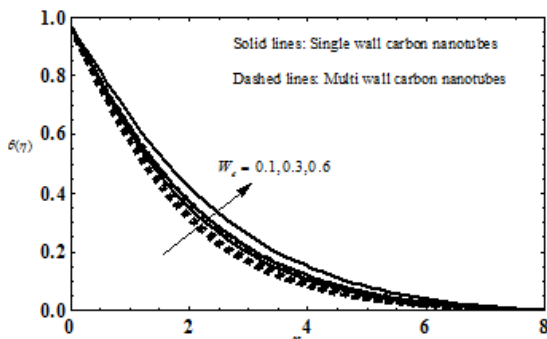


Fig. 11. Temperature profiles for different values of We .

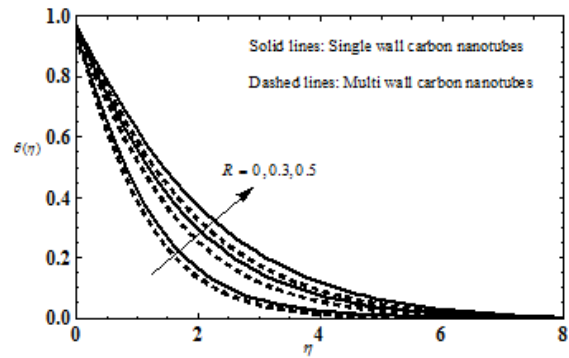


Fig. 12. Temperature profiles for different values of R .

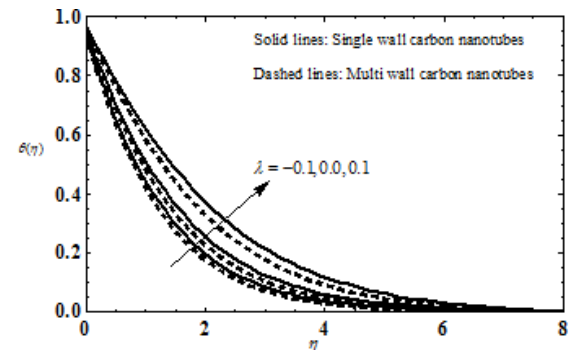


Fig. 13. Temperature profiles for different values of λ .

Radiation effect on $\eta(\theta)$ is shown in Fig. 12. An increase in the radiative heat transfer rises the warmth in the nanofluid. Physically, enhancing radiation releases more heat energy inside the flow, the same helps in rising the temperature of the tangent hyperbolic nanofluid. Temperature distribution for varying heat source/sink parameter is depicted in Fig. 13. An increase in λ reduces the temperature of the fluid. It is due to the logic that heat generated in the nanofluid is absorbed by the stretching sheet, thus reducing the warmth in the nanofluid.

Figs. 14 and 15 represent the Velocity and thermal slip effects on $f'(\eta)$ and $\theta(\eta)$. Physically, magnetic field together with slip effect acts as a retarding force. This retarding force can control the fluid's velocity which is useful in numerous applications such as magneto-hydrodynamic power generation and electromagnetic coating of wires and metal. As expected, escalating Navier slip parameter (β) values depresses the momentum distribution at the free stream. An increase in the thermal slip parameter (δ) decreases the thermal boundary layer thickness.

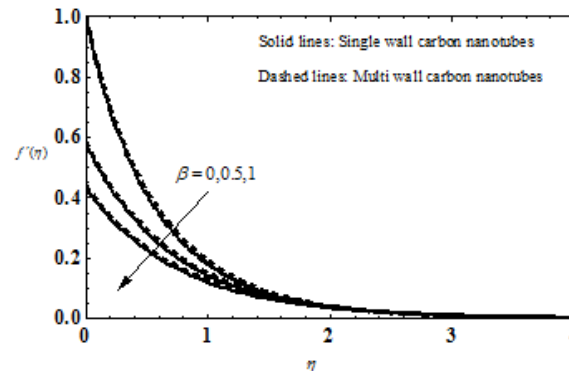


Fig. 14. Velocity profiles for different values of β .

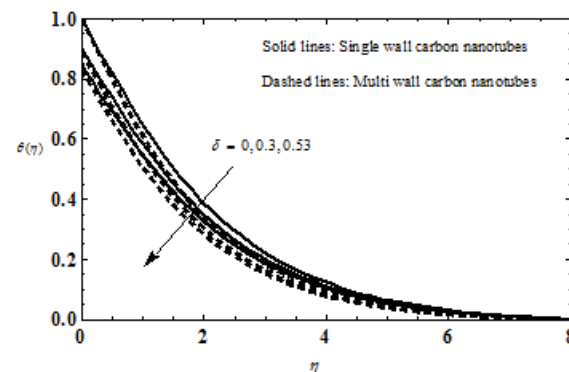


Fig. 15. Temperature profiles for different values of δ .

Therefore, decreasing the temperature of the nanofluid. It is because of the reason that a small amount of heat is swapped away by fluid from the sheet.

The influence of various governing physical parameters on the surface skin friction and rate of heat transfer are shown in Figs. 16-22. The variations of surface skin friction versus the CNT volume fraction for different values of aligned magnetic field is shown in Fig. 16. It is clear that the surface skin friction rate decreases with an increase in volume fraction of carbon nanotubes. Also it is evident that the surface skin friction increases for higher values of aligned magnetic field and the MWCNT have higher values than SWCNT. From Fig. 17, it is seen that the behaviour of skin friction decreases with an increase in nanoparticle volume fraction simultaneously. It is evident that the skin friction increases with an increase in power law index n . Also it is clear that the values of surface skin friction have higher values in the case of MWCNT's than the SWCNT's. The same behaviour is noticed with an increase in Weissenberg number We as shown in Fig. 18. Fig. 19 shows the surface skin friction against the volume fraction parameter ϕ in the presence of velocity slip parameter β . It is clear from this that the surface skin friction decreases with an increase in volume fraction. Also it is noticed that the skin friction increases with the higher values of slip parameter β and initially single-wall carbon nano tubes have higher values than multi-wall carbon nano tubes; then it shows opposite for away from the surface.

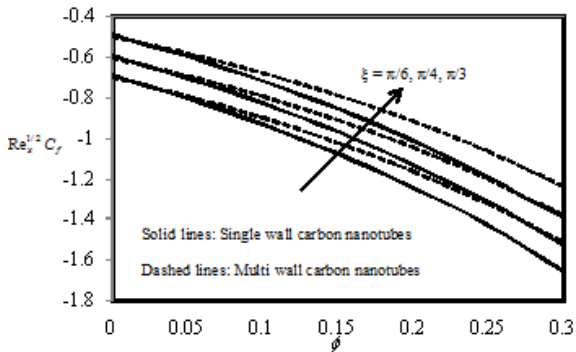


Fig. 16. Surface skin friction versus volume fraction for different values of ξ .

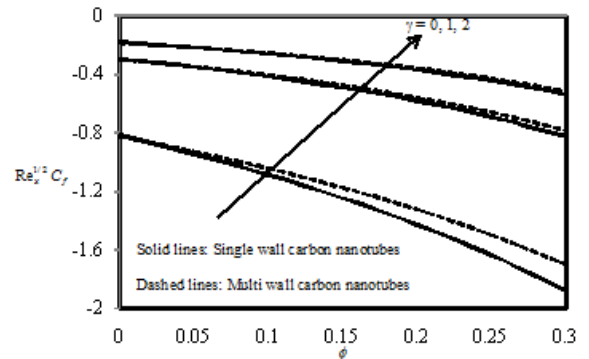


Fig. 17. Surface skin friction versus volume fraction for different values of γ .

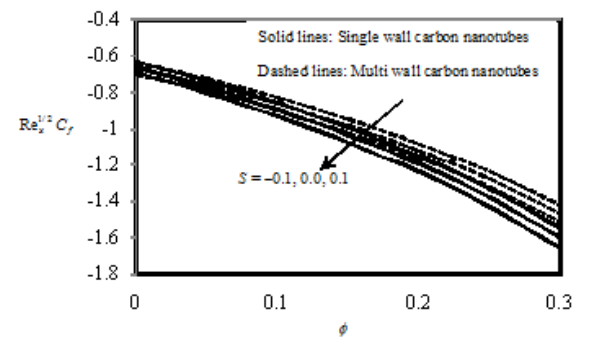


Fig. 18. Surface skin friction versus volume fraction for different values of S .

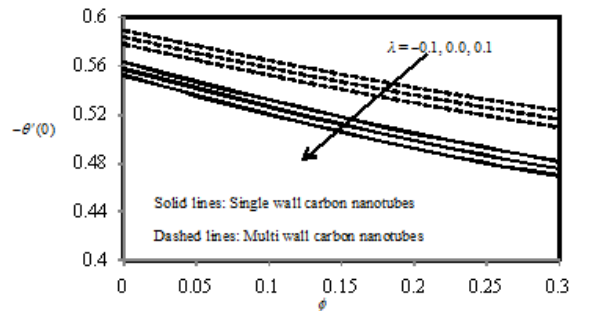


Fig. 19. Heat transfer rate versus volume fraction for different values of λ .

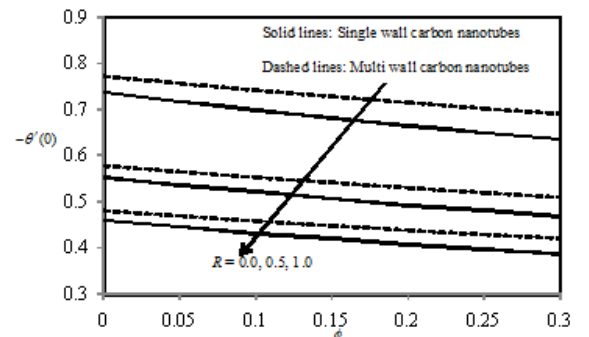


Fig. 20. Heat transfer rate versus volume fraction for different values of R .

The heat transfer rate at the surface decreases with an increase in the nano fluid volume fraction in the presence of radiation parameter R. Also it is evident that rate of heat transfer decreases with an increase in radiation parameter as shown in Fig. 20. The variations in the rate of heat transfer against the volume fraction of carbon nanotubes for different values of heat generation or absorption are shown in Fig. 21. The rate of heat transfer decreases with an increase in volume fraction in case of absorption and it shows an opposite behaviour in case of generation. Also it is evident that the rate of heat transfer decreases for increasing the values of heat generation or absorption and SWCNT dominates the MWCNT.

The rate of heat transfer at the surface against the volume fraction of carbon nano tubes for various values of temperature slip is shown in Fig. 22. From this, it is observed that the rate of heat transfer increases with an increase in volume fraction. Also it is noticed that the rate of heat transfer decreases for higher values of slip parameter δ .

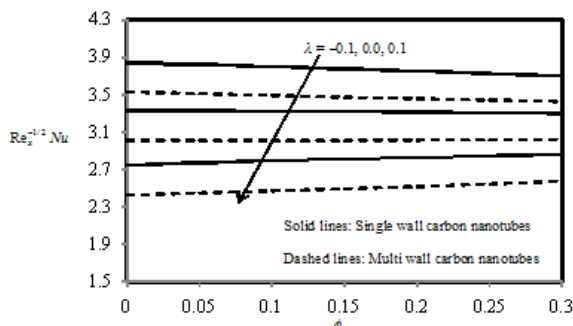


Fig. 21. Heat transfer rate versus volume fraction for different values of λ .

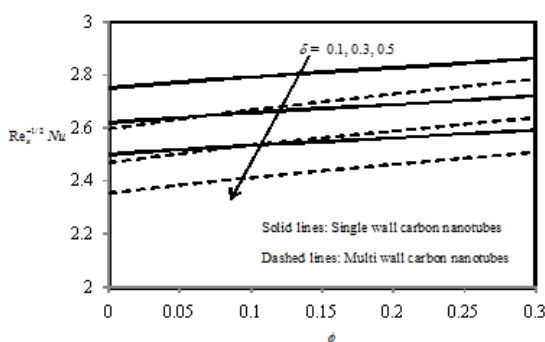


Fig.22. Heat transfer rate versus volume fraction for different values of δ

5. Conclusions

A mathematical model has been framed to study the influence of aligned magnetic field and slip effects on the boundary layer flow of carbon nanotubes past a vertical stretching sheet with thermal radiation and heat source or sink. From the investigation, the following summary can be drawn:

- The nanofluids with SWCNTs have higher effective thermal conductivities as compared to that having MWCNTs.
- The enhancement of heat transfer rate is seen with the increasing volume fraction of nanoparticles which was our main target because the purpose of adding nanoparticles to our working fluid is to enhance its rate of heat transfer and to make it useful for the practical purpose.
- Shear stress drops for the escalating volume fraction of CNTs while it accelerates for accelerating fluid parameter / Weissenberg number. MWCNTs profiles are elevating than SWCNTs.
- Heat transfer rate falls for rising radiative heat transfer parameter or heat source/sink parameter or thermal slip parameter.
- Skin friction drops for elevating aligned Lorentzian force or CNT volume fraction. MWCNTs dominate SWCNTs.

References

[1] S. U. S. Choi, “Nanofluids: from vision to reality through research”, *J. Heat Transfer*, Vol. 131, No. 3, 033106 (9 pages), (2009).

[2] M. Chandrasekar, and M.S. Kasi Viswanathan, “Analysis of heat and mass transfer on MHD flow of a nanofluid past a stretching sheet”, *Procedia Eng.*, Vol. 127, pp.493-500, (2015).

[3] T. Hayat, M. Rashid, M.Imtiaz, and A. Alsaedi, “Magnetohydrodynamic (MHD) stretched flow of nanofluid with power-law velocity and chemical reaction”, *AIP Adv.*, Vol. 5, No. 11, pp.117-121, (2015).

- [4] R. S. R. Gorla and B. Vasu, “Unsteady convective heat transfer to a stretching surface in a non-Newtonian nanofluid”, *J. Nanofluids*, Vol. 5, No. 4, pp. 581-594, (2016).
- [5] P. K. Kameswaran, B. Vasu, P. V. S. N. Murthy and Rama S. R. Gorla, “Mixed Convection from a Wavy Surface Embedded in a Thermally Stratified Nanofluid saturated Porous Medium with non-Linear Boussinesq Approximation”, *Int. Commun Heat Mass Transfer*, Vol. 77, pp.78-86, (2016).
- [6] R. Ul Haq, Z. Hayat Khan and W. A. Khan, “Thermophysical effects of carbon nanotubes on MHD flow over a stretching surface”, *Physica E*, Vol. 63, pp.215-222, (2014).
- [7] A. Waqar, I. Khan, I. Richard Culham and R. UlHaq, “Heat transfer analysis of MHD water functionalized carbon nanotube flow over a static/moving wedge”, *J. Nanomater*, ID 934367, 13 pages, (2015).
- [8] W. Khan, Z. Khan and M. Rahi, “Fluid flow and heat transfer of carbon nanotubes along a flat plate with Navier slip boundary”, *Appl. Nano Sci.*, Vol. 4, pp.633–641, (2014).
- [9] R. Ul Haq, S. Nadeem, Z. H. Khan and N. F. M. Noor, “Convective heat transfer in MHD slip flow over a stretching surface in the presence of carbon nanotubes”, *Physica B*, Vol. 457, pp.40–47, (2015).
- [10] R. Ul Haq, Z. H. Khan and W. A. Khan , “Thermo physical effects of carbon nanotubes on MHD flow over a stretching surface”, *Physica E*, Vol. 63, pp. 215–222, (2014).
- [11] P. Sreenivasulu and T. Poornima, “Magnetohydrodynamic boundary layer flow of a dissipating nanofluid past an exponential stretching sheet with convective boundary condition”, *Mathematical Sciences International Research Journal*, Vol. 4, No. 2, pp. 288-292, (2015).
- [12] T. Poornima, N. Bhaskar Reddy and P. Sreenivasulu, “Temperature dependent viscosity effect on MHD mixed convective dissipating flow of cylinder shaped Cu-water nanofluid past a vertical moving surface”, *Proc. of Int. Conference on Frontiers in Mathematics, Gauhati University, Guwahati, Assam, India.*, pp.235-242, (2015).
- [13] T. Hayat, I. Ullah, A. Alsaedi and M. Farooq, “MHD flow of Powell-Eyring nanofluid over a non-linear stretching sheet with variable thickness”, *Results Phys*, Vol. 7, pp. 189–196, (2017).
- [14] B. Vasu, O. A. Béǵ and V. R. Prasad, “Numerical study of mixed bioconvection in porous media saturated with nanofluid containing oxytactic microorganisms”, *J. Mech. Med. Biol.*, Vol. 13, No. 4, pp. 1350067 (2013).
- [15] S. C. Reddy, K. Naikoti and M. M., Rashidi, “MHD flow and heat transfer characteristics of Williamson nanofluid over a stretching sheet with variable thickness and variable thermal conductivity”, *Transactions of A. Razmadze Mathematical Institute*, Vol. 171, No. 2, pp. 195–211, (2017).
- [16] R. E. Ergun, C. W. Carlson, J. P. McFadden, F. S. Mozer, L. Muschietti, I. Roth and R. J. Strangeway, “Debye-Scale plasma structures associated with magnetic-field-aligned electric fields”, *Phys. Rev. Lett.*, Vol. 81, No. 4, 826, (1998).
- [17] M. M. Rashidi, N. Vishnu Ganesh, A. K. Abdul Hakeem and B. Ganga, “Buoyancy effect on MHD flow of nanofluid over a stretching sheet in the presence of thermal radiation”, *J. Mol. Liq.*, Vol. 198, pp.234-238, (2014).
- [18] M. A. Wahed and M. Akl, “Effect of hall current on MHD flow of a nanofluid with variable properties due to a rotating disk with viscous dissipation and nonlinear thermal radiation”, *AIP Adv.*, Vol. 6, No.9, 095308-1-14, (2016).

- [19] D. Lu, M. Ramzan, N. Ul Huda, J. D. Chung and U. Farooq, “Nonlinear radiation effect on MHD Carreau nanofluid flow over a radially stretching surface with zero mass flux at the surface”, *Sci. Rep.*, Vol. 8, 3709, pp.1-17, (2018).
- [20] T. Poornima, N. Bhaskar Reddy and P. Sreenivasulu, “Slip Flow of Casson Rheological Fluid under Variable Thermal Conductivity with Radiation”, *Heat Tran Asian Res*, Vol. 44, No. 8, pp.718-737, (2015).
- [21] N. Bhaskar Reddy, T. Poornima and P. Sreenivasulu, “Radiative heat transfer effect on MHD slip flow of Dissipating Nanofluid past an exponential stretching porous sheet”, *Int. J. Pure Appl. Math.*, Vol. 109, No. 9, pp.134 – 142, (2016).
- [22] Y. B. Kho, A. Hussanan, M. K. A. Mohamed, N. M. Sarif, Z. Ismail and M. Z. Salleh, “Thermal radiation effect on MHD flow and heat transfer analysis of Williamson nanofluid past over a stretching sheet with constant wall temperature”, *Journal of Physics: Conf. Ser.*, Vol. 890, No. 1, 012034, (2017).
- [23] T. Poornima and P. Sreenivasulu, “Radiation effects on MHD convective boundary layer flow of Eg-based Cu nanotubes due to an extensible moving surface”, *Mathematical Sciences International Research Journal*, Vol. 4, No. 2, pp. 293-297, (2015).
- [24] T. Hayat, M. Ijaz Khan, M. Waqas, A. Alsaedi, and M. Farooq, “Numerical simulation for melting heat transfer and radiation effects in stagnation point flow of carbon–water nanofluid”, *Comput. Methods Appl. Mech. Engg*, Vol. 315, pp. 1011–1024, (2017).
- [25] I. Rashid, R. Ul Haq, and Q. M. Al-Mdallal, “Aligned magnetic field effects on water based metallic nanoparticles over a stretching sheet with PST and thermal radiation effects”, *Physica E*, Vol. 89, pp. 33-42, (2017).
- [26] A. Hussain, M.Y. Malik, T. Salahuddin, A. Rubab and M. Khan, “Effects of viscous dissipation on MHD tangent hyperbolic fluid over a nonlinear stretching sheet with convective boundary conditions”, *Results Phys.*, Vol. 7 pp. 3502–3509, (2017).
- [27] Z. Ullah, and G. Zaman, “Lie group analysis of magnetohydrodynamic tangent hyperbolic fluid flow towards a stretching sheet with slip conditions”, *Heliyon*, Vol. 3, No. 11, e00443, pp. 1-15, (2017).
- [28] N. S. Akbar, S. Nadeem, R. U. Haq and Z. H. Khan, “Numerical solutions of magnetohydrodynamic boundary layer flow of tangent hyperbolic fluid towards a stretching sheet”, *Indian J. Phys*, Vol. 87, No. 11, pp. 1121-1124, (2013).
- [29] G. T. Thammanna, B. J. Gireesha and B. Mahanthesh, “Partial slip and Joule heating on magnetohydrodynamic radiated flow of nanoliquid with dissipation and convective condition”, *Results Phys.*, Vol. 7, pp. 2728-2735, (2017).
- [30] M. Naseer, M. Y. Malik, S. Nadeem and A. Rehman, “The boundary layer flow of hyperbolic tangent fluid over a vertical exponentially stretching cylinder”, *Alex. Eng. J.*, Vol. 53, pp.747–750, (2014).
- [31] N. Sandeep, “Effect of aligned magnetic field on liquid thin film flow of magnetic-nanofluids embedded with graphene nanoparticles”, *Adv Powder Technol*, Vol. 28, No. 3, pp. 865-875, (2017).
- [32] M. Sailaja, R. Hemadri Reddy, R. Saravana and K. Avinash, “Aligned magnetic field effect on unsteady liquid film flow of Casson fluid over a stretching surface”, *Mate. Sci. Eng.*, Vol. 263, No. 6, pp.1-8, (2017).
- [33] N. S. Arifin, S. M. Zokri, A. R. M. Kasim, M. Z. Salleh, N. F. Mohammad and W. N. S. W. Yusoff, “Aligned magnetic field of two-phase mixed convection flow in dusty Casson fluid over a stretching sheet with Newtonian heating”, *J. Phys: Conf. Ser.*, Vol. 890, No. 1, pp. 1-6, (2017).

- [34] M. Rashidi, M. Babu, M. Jayachandra, N. Sandeep and M. Ali, "MHD squeezing flow of nanofluid between parallel plates in the presence of aligned magnetic field", *J. Compu. Theor. Nanos.*, Vol. 13, No. 11, pp. 8700-8708(9), (2016).
- [35] I. Waini, N. A. Zainal and N. S. Khashi'ie, "Aligned magnetic field effects on flow and heat transfer of the upper-convected Maxwell fluid over a stretching/shrinking sheet", *MATEC Web Conf.*, Vol. 97, 01078, 10 pages, (2017).
- [36] G. P. Ashwin kumar, C. Sulochana and S. P. Samrat, "Effect of the aligned magnetic field on the boundary layer analysis of magnetic-nanofluid over a semi-infinite vertical plate with ferrous nanoparticles", *Multidiscip. Model. Mater. and Struct*, Vol. 14, No. 3 pp.497-515, (2017).
- [37] Q. Z. Xue, "Model for thermal conductivity of carbon nanotube-based composites", *Physica B*, Vol. 368, No.1-4, pp. 302–307, (2005).
- [38] S. Mukhopadyaya, G. C. Layek and S. A. Samad, "Study of MHD boundary layer flow over a heated stretching sheet with variable viscosity", *Int. J. Numer. Method. H*, Vol. 48, No. 21-22, pp.4460-4466, (2005).
- [39] K. Uma, G. Maheswararao and Koteswara rao, "Boundary layer flow of MHD tangent hyperbolic fluid past a vertical plate in the presence of thermal dispersion using spectral relaxation method", *Int. J. Comput. Eng. Res.*, Vol. 07, No. 06, pp.28-41, (2017).

How to cite this paper:

P. Sreenivasulu, B. Vasu, T. Poornima and N. Bhaskar Reddy, "Inclined lorentzian force effect on tangent hyperbolic radiative slip flow imbedded carbon nanotubes: lie group analysis", *Journal of Computational and Applied Research in Mechanical Engineering*, Vol. 10, No. 1, pp. 85-99, (2020).

DOI: 10.22061/jcarme.2018.4220.1508

URL: http://jcarme.sru.ac.ir/?_action=showPDF&article=900

